Determination of an Optimal Potential Window for Catalysis by *E. coli* Dimethyl Sulfoxide Reductase and Hypothesis on the Role of Mo(V) in the Reaction Pathway†

Kerensa Heffron,‡ Christophe Léger,‡ Richard A. Rothery,§ Joel H. Weiner,§ and Fraser A. Armstrong*,‡

Inorganic Chemistry Laboratory, Oxford University, South Parks Road, Oxford, OX1 3QR, United Kingdom, and Department of Biochemistry, 474 Medical Sciences Building, University of Alberta, Edmonton, Alberta T6G 2H7, Canada

Received October 23, 2000; Revised Manuscript Received January 10, 2001

ABSTRACT: Protein film voltammetry (PFV) of *Escherichia coli* dimethyl sulfoxide (DMSO) reductase (DmsABC) adsorbed at a graphite electrode reveals that the catalytic activity of this complex Mo-pterin/Fe-S enzyme is optimized within a narrow window of electrode potential. The upper and lower limits of this window are determined from the potential dependences of catalytic activity in reducing and oxidizing directions; i.e., for reduction of DMSO (or trimethylamine-*N*-oxide) and oxidation of trimethylphosphine (PMe_3). At either limit, the catalytic activity drops despite the increase in driving force: as the potential is lowered below −200 mV (pH 7.0−8.9), the rate of reduction of DMSO decreases abruptly, while for PMe_3, an oxidative current is observed that vanishes as the potential is raised above +20 mV (pH 9.0). Analysis of the waveshapes reveals that both activity thresholds result from one-electron redox reactions that arise, most likely, from groups within the enzyme; if so, they represent "switches" that reflect the catalytic mechanism and may be of physiological relevance. The potential window of activity coincides approximately with the appearance of the Mo(V) EPR signal observed in potentiometric titrations, suggesting that crucial stages of catalysis are facilitated while the active site is in the intermediate Mo(V) oxidation state.

When grown anaerobically in the presence of dimethyl sulfoxide (DMSO),[1] *Escherichia coli* expresses a menaquinol:DMSO reductase, DmsABC. This membrane-bound oxidoreductase couples the two-electron oxidation of menaquinol (MQH_2) in the cytoplasmic membrane ($E_{m,7} = -70$ mV) with the reduction of DMSO to dimethyl sulfide (DMS) ($E_{m,7} = +160$ mV) (*1*−*4*). DmsABC is one of an emerging family of bacterial [Fe-S]-molybdoenzymes [others include formate dehydrogenase (FdnGHI) and respiratory nitrate reductase (NarGHI) (*5*−*7*)] which catalyze electron transport between the membrane-bound quinone pool and aqueous substrates. As depicted in Figure 1, DmsABC comprises three subunits: the catalytic subunit DmsA (85.8 kDa) (*8*) is the site of DMSO reduction and contains a molybdenum atom coordinated by dithiolene linkages to two molybdopterin guanine dinucleotides, i.e., Mo-bisMGD; the electron-transfer subunit DmsB (23.1 kDa) contains four [4Fe-4S] clusters; by contrast, the third subunit DmsC (30.8 kDa) is located within the membrane and contains the MQH_2 binding site (*9*−*11*). Figure 1 also shows the reduction potentials of the centers at pH 7 ($E_{m,7}$), as determined by EPR (*9*, *12*, *13*). Values for the Mo-active site are those determined in this study (vide infra). The electron-transfer pathway has been proposed (*14*) on the basis of (i) a conformational link between the MQH_2 binding site and the $[4Fe\text{-}4S]^{2+/+}$ cluster with $E_{m,7} = -50$ mV (*11*); (ii) a strong spin−spin interaction of this cluster and the one with $E_{m,7} = -120$ mV (*11*); and (iii) a strong spin−spin interaction between the latter cluster and the S = 1/2 Mo(V) form of the active site (*14*). The two remaining [4Fe-4S] clusters have much lower reduction potentials ($E_{m,7} = -240$ and −330 mV) (*9*).

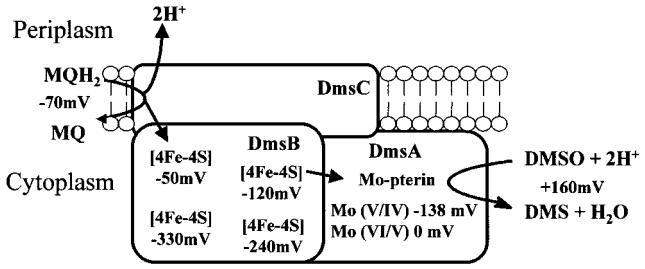

FIGURE 1: Schematic model of DMSO reductase showing the reduction potentials of the [Fe-S] clusters (*9*) and the Mo active site (this study) and the proposed electron-transfer pathway through the enzyme (*9*, *11*, *14*).

† The authors acknowledge the UK EPSRC and BBSRC (Grant number 43/B10492), and the Human Frontier Science Program Organization (Grant number RG0170/200-M) for support.

* To whom correspondence should be addressed. Department of Chemistry, Inorganic Chemistry Laboratory, Oxford University, South Parks Road, Oxford, OX1 3QR, UK. Telephone: (01865) 272647. Fax: (01865) 272690. E-mail: fraser.armstrong@chem.ox.ac.uk.

‡ Oxford University.

§ University of Alberta.

[1] PFV, protein film voltammetry; DMSO, dimethyl sulfoxide; DmsABC, *Escherichia coli* DMSO reductase; TMAO, trimethylamine-*N*-oxide; PMe_3, trimethylphosphine; EPR, electron paramagnetic resonance; MQH_2, menaquinol; DMS, dimethyl sulfide; $E_{m,7}$, midpoint reduction potential at pH 7; *Rh.*, *Rhodobacter*; Mo-bisMGD, molybdo-bis(molybdopterin guanine dinucleotide); SDS, sodium dodecyl sulfate; SCE, saturated calomel electrode; SHE, standard hydrogen electrode; PGE, pyrolytic graphite edge; PGB, pyrolytic graphite basal plane; $OPMe_3$, trimethylphosphine oxide.

10.1021/bi002452u CCC: $20.00
Published on Web 02/10/2001

Recent studies on the DMSO reductases from *Rhodobacter capsulatus* and *Rh. sphaeroides* have indicated that the active site undergoes complex structural transformations. These single-subunit enzymes contain no cofactors besides the active site oxo-Mo center, and show 25−32% sequence identity and 35−41% similarity with the *E. coli* DmsA subunit (*14*). The crystal structures of the *Rhodobacter* enzymes have been solved (*15*−*20*), and although a consensus on the active site structure is still lacking, the Mo appears to be coordinated by a serine (Ser176 in the case of the *E. coli* DmsABC) (*13*) and up to four thiolene sulfurs from the two MGD groups. Additional information on the active sites has been obtained from spectroscopy: for example, resonance Raman studies of *Rh. capsulatus* DMSO reductase and of *Rh. sphaeroides* biotin sulfoxide reductase each indicate that both pairs of dithiolenes remain attached to Mo throughout the catalytic cycle (*21*, *22*). Results of recent X-ray absorption and Mo(V) EPR studies (*23*) are in accordance with those from resonance Raman; however, they also reveal that reduction by DMS or dithionite produces states with four or three coordinated sulfur atoms, respectively. Adams et al. have reported a modified form of *Rh. capsulatus* DMSO reductase, $DMSOR_{mod}$, which arises after prolonged exposure to DMS (*24*). This form is inactive toward oxidation of DMS, and although DMSO reduction appears unaffected, the assay procedure (using reduced methyl viologen and DMSO) is essentially identical to the "redox-conditioning" procedure that regenerates the active form of the enzyme. Recent crystallographic studies have shown that aerobic exposure to Na^+-HEPES buffer alters the coordination sphere of Mo in *Rh. capsulatus*: a pair of thiolate ligands dissociates, leading to loss of activity in the backward assay (*25*). This is the first clear evidence that dissociation of sulfur ligands is not part of the catalytic cycle but is an artifact.

These studies reveal multiple structural states of the Mo-site that are not equally active. The Mo-bisMGD cofactor is indeed capable of complex redox chemistry: apart from formal changes in Mo oxidation state between IV, V, and VI, each pterin may exist in at least two oxidation states (the dihydro and oxidized states) (*26*), with the possibility also of tetrahydro and radical species (*27*). So far, the role of pterin redox states has received little attention, and even if the pterin does not undergo formal changes in oxidation state during catalysis, its status throughout is still difficult to establish. Furthermore, a dithiolene group could dissociate from the Mo (*25*) and undergo electron-transfer itself to give a thiyl radical (*28*) or disulfide (*24*).

Although the concept of pH optima for enzyme activity is well established, the possibility that activity may be optimized within a finite (and perhaps narrow) range of electrochemical potential has not been well explored. While pH optima give mechanistic information on protonation equilibria during catalysis, potential optima inform on the roles played by different oxidation states of redox-active sites. Certain redox transitions may regulate electron flow to or from the active site or may modulate catalytic activity in some other way; for example, substrate binding or atom transfer may occur only when the active site is in a certain oxidation state. These relationships are difficult to observe by conventional techniques but can be revealed by protein film voltammetry (PFV), due to its ability to measure subtle changes in catalytic activity as the electrode potential is varied (*29*−*33*).

In PFV, a redox protein is immobilized on a "friendly" electrode surface and electron-transfer reactions are induced, controlled, and monitored under precise conditions of electrode potential (*29*, *34*). Immobilization removes complications from sluggish protein diffusion in solution and allows direct control and observation of redox activity. Provided interfacial electron transfer is rapid (electrons are effectively "on-tap") and the enzyme retains its native properties, many properties of the system can be studied. In the absence of substrate and with sufficiently high electrode surface coverage, peak-like signals may be observed due to reversible electron exchange between enzyme and electrode, corresponding to oxidation and reduction of individual redox groups within the enzyme. Upon adding substrate, these "non-turnover" peaks transform to sizable waves as the electrode delivers or receives the electrons required for catalytic cycles; furthermore, substrate supply can be controlled by rotating the electrode. Since current equates directly to rate and hence to turnover number, the relationships between driving force (potential) and catalytic activity can be explored. Catalysis may still be studied if coverage is too low to observe non-catalytic signals; as for succinate dehydrogenase, where the unusual shape of the catalytic voltammetry reveals the relationship between the redox status of the enzyme and catalytic efficiency (*31*, *35*, *36*).

Here we present the results from a PFV study of *E. coli* DmsABC adsorbed from detergent-solubilized aqueous solution at edge or basal plane pyrolytic graphite electrodes. An intriguing potential dependence is observed in both oxidizing and reducing directions, revealing an optimum potential-window for catalytic activity. The origin of this effect and wider implications for Mo-enzyme catalysis are discussed.

EXPERIMENTAL PROCEDURES

Preparation of Enzyme Samples. Wild-type DmsABC was expressed in *E. coli* strain HB101 that had been transformed with plasmid pDMS160 (*37*) and grown anaerobically on a glycerol-fumarate minimal medium (*38*). The enzyme was isolated in the presence of DMSO according to the method of Cammack and Weiner (*9*), using Triton X-100 as detergent. Protein concentrations were determined using a modified Lowry assay with a bovine serum albumin standard (*1*), and reductase activity was assayed with trimethylamine-*N*-oxide (TMAO) as electron acceptor and lapachol as electron donor (*39*). Sample purity was assessed by SDS−polyacrylamide gel electrophoresis. Isolated enzyme had a specific activity of 1.4 μmol of lapachol oxidized min^{-1} (mg of protein)$^{-1}$. The purified enzyme, at a concentration of approximately 80 μM, was stored as pellets under liquid nitrogen.

For greater protein stability, the buffers used to purify and store enzyme contained DMSO at 0.15% w/v. Where necessary, DMSO was removed, as far as possible, immediately before experiments by gel filtration on a PD-10 column (Amersham Pharmacia Biotech).

Voltammetry. Voltammetry was performed with an Autolab potentiostat PGSTAT 10 or 20 (Eco Chemie, Utrecht, The Netherlands) equipped with an analogue or digital scan generator and ECD module and controlled by GPES software

(Eco Chemie). Data analysis was carried out using an in-house program: where necessary, the voltammetric data were smoothed using a fast Fourier transform procedure, and then the non-faradaic background was removed by subtracting a second-order polynomial function. Experiments were carried out anaerobically at 25 °C in a glovebox (Vacuum Atmospheres) with O_2 < 2 ppm. A thermostated three-electrode glass cell or multipot cell, each with a Luggin sidearm housing a saturated calomel electrode (SCE), were used as described previously and housed in a Faraday cage to minimize electrical noise (*30*, *34*). All potentials have been corrected to the standard hydrogen electrode (SHE) using $E_{SHE} = E_{SCE} + 241$ mV at 25 °C (*40*). Pyrolytic graphite edge (PGE) or basal plane (PGB) working electrodes were constructed as described previously (*30*, *34*).

All solutions were prepared with purified water (Millipore, 18 MΩ.cm). Most voltammetry experiments utilized a mixed buffer system consisting of 20 mM in each of MES [2-(*N*-morpholino)ethanesulfonic acid], TAPS [*N*-tris(hydroxymethyl)methyl-3-amino-propanesulfonic acid], HEPES [*N*-(2-hydroxyethyl)piperazine-*N*′-2-ethanesulfonic acid], and CHES [2-(*N*-cyclohexyl-amino)ethanesulfonic acid] (all purchased from Sigma). Solutions included 0.1 M NaCl (BDH) as additional supporting electrolyte, 100 μM EGTA [ethylene glycol-bis(b-aminoethyl ether)-*N*,*N*,*N*′,*N*′-tetraacetic acid] (Sigma), and polymyxin B sulfate (Sigma) (200 μg/mL) to stabilize the protein film on the electrode. The final pH was adjusted using concentrated HCl and NaOH (BDH). Concentrated stock solutions of substrates DMSO (Sigma), TMAO (Sigma), DMS (Aldrich), PMe_3 (Fluka), and $OPMe_3$ (Alfa) were made up in pH-buffered solutions and added to the cell to give the desired final concentrations. In the cases of PMe_3 and DMS, these stock solutions were used immediately.

Prior to each experiment, the PGE electrode was prepared by polishing with an aqueous alumina slurry (1 μm, Buehler) then sonicating for 15 s. The PGB electrode, in which the graphite block is housed within a sheath of silicon rubber, was prepared by cleaving along the plane with a scalpel to expose a fresh surface.

In typical experiments, an aliquot of concentrated DmsABC solution was added to the cell solution to give a final concentration of approximately 1 μM. To develop a protein film, a freshly prepared electrode was introduced to the cell and the potential was cycled between −560 and +140 mV vs SHE at 10 mV/s until the catalytic current was maximized (this took at least 20 min, after which time the current began to decrease). Greater stability was observed when using a PGE electrode instead of PGB; hence, experiments were carried out at a PGE electrode unless otherwise stated.

EPR Spectroscopy. EPR spectra were recorded using a Bruker ESP300 spectrometer equipped with an Oxford Instruments ESR-900 flowing helium cryostat. Potentiometric titrations were carried out as previously described, with 150 μL samples being extracted from the titrations into quartz EPR tubes (3 mm internal diameter) (*11*, *14*). Potentiometric titrations were carried out on DmsABC-enriched membranes at a protein concentration of approximately 30 mg/mL in the following buffers containing 5 mM EDTA and 100 mM buffer: MES (pH 6.0), MOPS ([2-(*N*-morpholino)propanesulfonic acid], pH 7.0), Tricine (pH 8.0), or CHES (pH 9.0), each adjusted to the desired pH with KOH. EPR spectra were recorded at 75 K at a microwave power of 2 mW and a modulation amplitude of 3.8 G_{pp}. Titration data were extracted from the intensity of the $g = 1.98$ peak-trough of each spectrum as previously described (*13*, *14*).

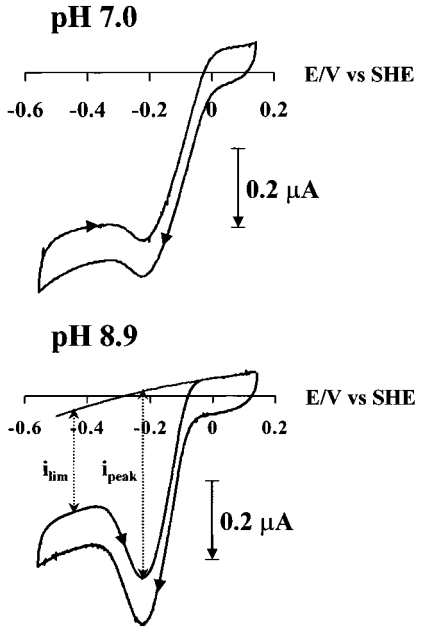

FIGURE 2: Catalytic voltammetry of adsorbed DMSO reductase at pH 7.0 and pH 8.9. The films were adsorbed from ∼1 μM DmsABC solution, containing 50 mM buffer, 20 mM DMSO, and 20 μg/mL polymyxin. Total cell volume 1 mL, temperature 25 °C, scan rate 5 mV/s. The background (in the absence of enzyme and substrate) is shown on the data at pH 8.9 in gray, and the measurement of i_{peak} and i_{lim} is indicated.

RESULTS

Reductive Catalysis. Figure 2 shows cyclic voltammograms measured at pH 7.0 and 8.9 using a stationary PGE electrode, after allowing adsorption of DmsABC from 1 μM solution, in the presence of 20 mM DMSO. In both cases, a large catalytic reduction current is observed, due to reduction of DMSO by the enzyme and regeneration of the reduced enzyme by the electrode. Thus electrons that are normally supplied by menaquinol in vivo are supplied instead by the electrode:

$$DMSO + 2H^+ + 2e^- \rightarrow DMS + H_2O \qquad (1)$$

Catalytic reduction of DMSO is observed over the pH range of 5.5 to 9.5, and the waveforms exhibit an unusual potential dependence. Above 0 mV, no current is evident over that due to background capacitance; then as the potential is taken to more negative values, a catalytic current flows. This current increases to a maximum value beyond which it drops abruptly, giving rise to a peak that is observed irrespective of the direction of scanning, and which is much more pronounced at higher pH (note the term "peak" is used in voltammetry to describe maxima for both oxidation and reduction currents). The effect is similar to observations made on some other enzymes, notably, succinate dehydrogenase and Ni-Fe hydrogenase (*31*, *35*, *36*, *41*, *42*). This behavior has been termed a "tunnel diode" effect because, like the electronic device of this name, there is a region of potential in which the current decreases with increasing bias (driving

force), i.e., equivalent to *negative* resistance. In molecular terms, the effect must arise from a redox transition that acts as a "switch" to modulate activity.

This effect is due entirely to the catalytic activity of DmsABC, since in the absence of enzyme, no reduction of substrate is observed in the potential range −0.6 to +0.3 V vs. SHE. Without substrate (requiring prior removal of DMSO from the enzyme stock), no signals of any type were discernible above the background, indicating that the electroactive coverage must be very low (<1 pmol/cm^2) (*41*).

At high DMSO concentrations (20 mM) corresponding to approximately 100 K_M [K_M = 0.18 mM, pH 7.0, 30 °C, based on assays (*3*)], the enzyme is saturated with substrate. The limiting catalytic currents at low potentials display no dependence on electrode rotation rate, showing that there is no depletion of substrate at the electrode−solution interface. Under such conditions, the concentration of substrate presented to the enzyme is similar to that in bulk solution, and catalysis is not limited by its transport to the electrode surface. The voltammetry is independent of scan direction and scan rate up to around 50 mV/s, and thus is considered to be at steady-state.

At low DMSO concentrations ($\leq K_M$), the limiting current increases as the concentration of DMSO increases and depends on electrode rotation rate, as expected if substrate mass transport limits the reaction. However, this was only a qualitative observation since, although the catalytic current increases as the rotation rate is increased, the enzyme film was rapidly destabilized under rotating conditions. The catalytic response persisted if the electrode was then transferred to a cell solution containing DMSO but no enzyme, confirming that enzyme molecules are adsorbed. However, the stability of the protein film was poor over the entire pH range investigated. After attaining a maximum value, reduction currents typically decreased by 50% over the course of 15−20 min, although there was no change in waveshape.

It is known that DmsABC functions with a number of electron acceptors (*3*), including TMAO. Experiments with this substrate gave similar voltammetry to those with DMSO, with a reductive peak appearing at the same potential; however, higher substrate concentrations were required to reach saturating conditions, in accordance with the higher K_M and k_{cat} values [20.2 mM and 1203 s^{-1}, respectively, at 30 °C, pH 7 (*3*)].

Activity as a Function of pH. Since we were unable to observe non-catalytic signals from which coverage could be estimated, the absolute activity (i.e., a value of k_{cat}) could not be quantified. However, we were able to compare the relative activities over a range of pH. This was achieved by developing a film at pH 9.0 and then transferring the electrode to another solution at a different pH. Minor corrections for loss of electroactive enzyme were made where necessary, judged by comparing the currents obtained at pH 9.0 before and after the pH jump. This procedure was repeated for different pH values. On placing the electrode in an electrolyte at different pH, there was an instantaneous change in the limiting current and catalytic potential, which was fully reversed upon returning to pH 9.0. The adsorbed enzyme therefore adjusts rapidly and reversibly to the pH of the electrolyte. Figure 3, panel A, shows the ratio of the limiting current obtained at a particular pH to the limiting current at pH 9.0. The enzyme is most active at pH 6.0, with activity decreasing to 50% at pH 7.5. Similar experiments carried out after adsorbing the protein at pH 7.0 gave the same profile, although catalytic currents were smaller, showing that greater electroactive coverage is obtained at pH 9.0. Solution assays with lapachol as electron donor showed a similar trend in activity as a function of pH.

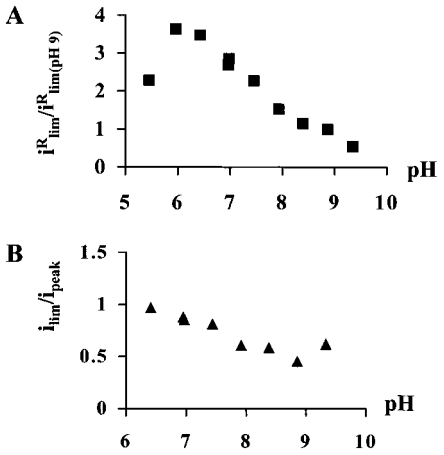

FIGURE 3: (a) Activity toward DMSO reduction, assessed as the limiting catalytic current at low potential, as a function of pH. These values are expressed as the ratios of the limiting catalytic currents at the given pHs to those observed at pH 9.0. (b) Ratio of i_{lim}/i_{peak} (as a measure of the extent of the switch) as a function of pH. Temperature 25 °C, scan rate 5 mV/s, 20 mM DMSO.

The catalytic waveshape changes as a function of pH. At pH 6.0 and below, the response is essentially sigmoidal, while at higher pH values the peak (as shown in Figure 2) becomes increasingly prominent. The effect of pH is indicated by the ratio of the limiting current at low potential, i^R_{lim}, to the peak current, i^R_{peak}, as shown in Figure 3, panel B.

Oxidative Catalysis. The results with DMSO (and TMAO) suggest the possibility that catalytic activity is linked to the oxidation level of a center in the enzyme (i.e., the Mo active site, vide infra). It was thus important to ascertain if the same characteristics are observed for catalysis in the oxidizing direction. DMSO reductase from *Rh. capsulatus* is known to function in a bidirectional manner, i.e., it also oxidizes DMS (*24*). However, the *E. coli* enzyme is not known to catalyze this reverse reaction, and there was no change in the voltammetry even with DMS in 1000-fold excess over DMSO. Therefore, the reduction of DMSO catalyzed by DmsABC at the electrode is unidirectional and, furthermore, is not inhibited by product. The unidirectionality is expected since the reduction potential of the DMSO/DMS couple at pH 7.0 (+160 mV) (*43*) is much higher than the potential (E^R_{cat}) at which catalysis is observed (approximately −100 mV at pH 7.0).

To investigate the potential-dependence of oxidizing activity, we required a substrate with a more negative reduction potential. We therefore examined the catalytic activity of adsorbed DmsABC toward the oxyphilic reagent trimethyl phosphine, PMe_3 (*44*). Figure 4 shows the voltammetry obtained at pH 9.0 in the presence of 10 mM PMe_3, corresponding to the following oxidation reaction:

$$PMe_3 + H_2O \rightarrow OPMe_3 + 2H^+ + 2e^- \qquad (2)$$

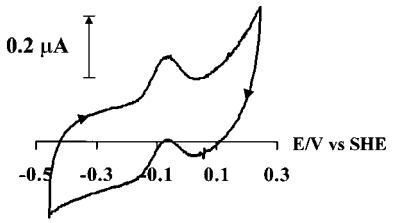

FIGURE 4: Catalytic oxidation of PMe_3 by adsorbed DMSO reductase at pH 9.0. The films were adsorbed from ~1 μM DmsABC solution containing 50 mM CHES, 10 mM PMe_3, and 20 μg/mL polymyxin. Total cell volume 1 mL, temperature 25 °C, and scan rate 20 mV/s.

No catalytic wave is observed in the absence of enzyme, although some direct oxidation of PMe_3 at the electrode surface is evident from the increased background current as the potential is raised. However, in the presence of enzyme, a positive current is observed due to catalytic oxidation of PMe_3. The waveform is not sigmoidal but is peak-like in both scan directions, showing that catalytic oxidation also displays a potential-dependent switch-off as the driving force (and potential) is raised. The switch-off is virtually total in this direction, and beyond 0 mV there is little discernible enzyme-mediated oxidation. Overall, the catalytic response is much weaker and less stable than for DMSO reduction (concentrations of PMe_3 greater than 5 mM were required to observe any catalytic current peak, which decreased by 50% within a few minutes), and no response was observed at pH 7.0. In addition, the substrate range was limited by its poor solubility (the maximum concentration possible being 50 mM). These problems meant we were unable to measure, reliably, how the current varies with substrate concentration. Additions of excess $OPMe_3$ (up to 20 mM) neither yielded any reduction current nor affected the oxidation peak.

Further Experiments to Determine the Origin of the Potential Dependence. Several experiments were designed to establish that the unusual potential dependence of catalytic activity is an intrinsic property of the enzyme and not an artifact resulting from potential-dependent surface interactions. Initially, the solution composition, expected to influence the interaction of the enzyme with the PGE surface, was changed. Exchanging the organic buffers for an inorganic buffer (borate) or substituting $NaClO_4$ for NaCl electrolyte gave identical results. Omitting polymyxin as coadsorbate produced the same current−potential response, although protein film stability was lower. The nature of the electrode surface was also varied. Experiments carried out at a PGB electrode gave voltammetry that was identical to, though less stable than, that obtained at PGE. No response was obtained using completely alternative electrodes such as indium tin oxide, bare gold, or a gold surface functionalized with a hexanethiol self-assembled monolayer (*45*).

Another attempt to verify the origin of the potential-dependent "switch" was made by studying the steady-state solution kinetics in a non-electrochemical experiment. In the case of succinate dehydrogenase, the behavior in the reduced benzyl viologen/fumarate assay (where the rate of reaction increases as benzyl viologen is consumed, and thus as the solution potential is raised) mirrors the "tunnel-diode" behavior observed electrochemically (*46*). It was thus expected that a similar result might be observed for DmsABC in assays in which the potential of the solution increases as the reduced electron donor is consumed. Such assays were performed at pH 9.0 with reduced lapachol, a menaquinol analogue, as the electron donor; however, we could detect no increase in rate as the reaction progressed.

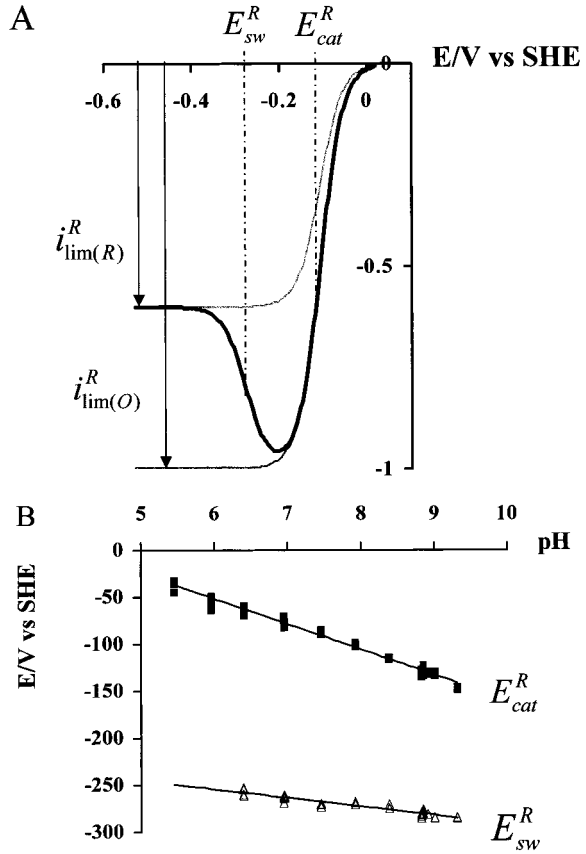

FIGURE 5: (A) Definition of the parameters used to characterize the shape of the voltammograms. E^R_{sw} is the potential of the switch observed during reduction; E^R_{cat} is the potential of the reductive catalytic wave; $i^R_{lim(R)}$ is the limiting catalytic current for the reduced form of the enzyme (after switching off); and $i^R_{lim(O)}$ is the limiting activity for the oxidized form. The gray lines indicate the hypothetical current profiles for the oxidized (more active) and reduced (less active) forms. The black line represents the observed catalytic profile as the enzyme converts between the two redox states. (B) pH dependence of the catalytic potential, E^R_{cat}, and the switch potential, E^R_{sw}, determined from the derivatives of the baseline-subtracted data (20 mM DMSO, scan rate 20 mV/s). The solid lines represent the lines of best fit through the data, revealing a pH dependence of −27 mV/pH for E^R_{cat} and −10 mV/pH for E^R_{sw}.

Modeling the Catalytic Waveforms. As indicated in Figure 5, panel A, the voltammetric wave can be characterized by two potentials, the half-wave potential of catalysis, E^R_{cat}, (the superscript R signifies this is for reduction) and the potential of the "switch", E^R_{sw}, responsible for interconversion between active and inactive (or less active) states. These parameters can be estimated from the positions of maximum gradient on either side of the peak in the $i(E)$ profile, i.e., where $d^2i/dV^2 = 0$. Figure 5, panel B, shows that in the pH range 5.5 to 9.5, the variation of E^R_{cat} with pH is approximately linear (slope −27 mV/pH unit) while E^R_{sw} changes less (−10 mV/pH unit).

The catalytic waveforms can be fitted to a Nernstian expression, although further parameters are required in addition to the potentials E^R_{cat} and E^R_{sw} defined in Figure 5, panel A. First, considering catalysis in the reductive direction

only, the sigmoidal waveform is described by an equation such as

$$\frac{i}{i^{R}_{lim}} = \frac{1}{1 + \exp\left[\frac{n^{R}_{cat}F(E - E^{R}_{cat})}{RT}\right]} \quad (3)$$

in which i is the current at potential E, i^{R}_{lim} is the limiting current at infinite overpotential, E^{R}_{cat} is the catalytic half-wave potential, and n^{R}_{cat} is an apparent number of electrons characterizing the width of the catalytic wave (the greater is n^{R}_{cat}, the steeper the wave). The terms F, R, and T have their usual meanings.

The "switch" can be accounted for in terms of a catalytically crucial group existing in two redox states, each having a specific activity characterized by the reductive limiting currents $i^{R}_{lim(O)}$ and $i^{R}_{lim(R)}$ for the oxidized and reduced forms, respectively. Provided equilibrium among redox centers is achieved over the entire potential range, the fraction of the enzyme in the less-active reduced form, ϕ, is given by

$$\phi = \frac{1}{1 + \exp\left[\frac{n^{R}_{sw}F(E - E^{R}_{sw})}{RT}\right]} \quad (4)$$

in which E^{R}_{sw} and n^{R}_{sw} are, respectively, the reduction potential and the number of electrons corresponding to the enzyme "switch" redox transformation.

The ratio of the activities of reduced and oxidized forms is defined as $(1 - q)$ in

$$(1 - q) = i^{R}_{lim(R)}/i^{R}_{lim(O)} \quad (5)$$

and the potential−current profile reads:

$$\frac{i}{i^{R}_{lim(O)}} = \frac{1 - q\phi}{1 + \exp\left[\frac{n^{R}_{cat}F(E - E^{R}_{cat})}{RT}\right]} \quad (6)$$

The catalytic reduction data were fitted according to eq 6 and adjusting $i^{R}_{lim(O)}$, q, E^{R}_{cat}, n^{R}_{cat}, E^{R}_{sw}, and n^{R}_{sw}. Typical fits at pH 7.0 and 8.9 are depicted in Figure 6. At pH 8.9, where the fit is closest to the data, the best values for n^{R}_{cat} and n^{R}_{sw} lie very close to 1.0 (typical deviation ± 0.1), while fixing both n values to 1 and adjusting the other four parameters gave the same results. The model therefore shows that the "switch" involves a one-electron redox process ($E_{m,9} = -284$ mV) to a reduced form that is approximately half as active as the oxidized form. The potentials E^{R}_{cat} and E^{R}_{sw} determined from the fit agree well with the values obtained from the derivative data. At pH 7.0, the fit is less satisfactory: close examination of the waveshape derivative (not shown) reveals a shoulder at −70 mV, suggesting that a process not accounted for by eq 6 is involved in catalysis at low pH. The parameters from the fits are summarized in Table 1.

The same treatment was applied to the results obtained with PMe_3 to give estimates of the potentials for E^{Ox}_{cat} and E^{Ox}_{sw} for catalysis in the oxidizing direction. It was assumed that the catalytic current decreases to zero at high potential,

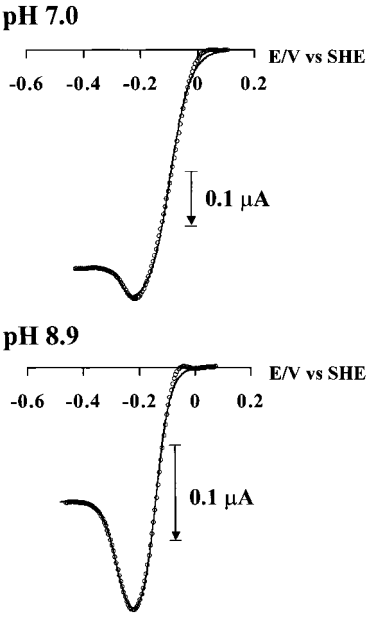

FIGURE 6: Baseline-subtracted data for catalytic reduction of DMSO at pH 7.0 and pH 8.9 (open circles), recorded in 20 mM DMSO at 20 mV/s. The black lines show the fit to eq 6: the results are summarized in Table 1.

Table 1: Summary of the Parameters Determined for Substrate Turnover Over a Range of pH Values

pH	n_{cat}	E_{cat} (mV)	n_{sw}	E_{sw} (mV)
		DMSO reduction:		
7.0	0.70 ± 0.05	−97 ± 3	*a*	−270 ± 10
7.9	0.90 ± 0.07	−109 ± 3	1.2 ± 0.3	−275 ± 10
8.9	1.00 ± 0.05	−140 ± 3	1.0 ± 0.1	−282 ± 5
		PMe_3 oxidation:		
8.9	1.3 ± 0.15	−112 ± 5	1.0 ± 0.1	−26 ± 5

[a] Not possible to determine with significant accuracy, as the switch is barely present.

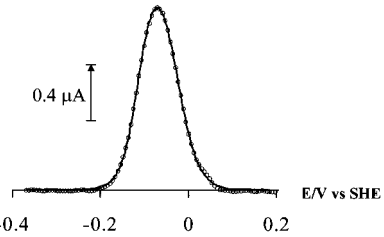

FIGURE 7: Baseline-subtracted data for catalytic oxidation of PMe_3 at pH 9.0 (open circles), recorded in 10 mM PMe_3 at 20 mV/s. The black line shows the fit to eq 7: the results are summarized in Table 1.

i.e., that the switch-off is total ($q = 1$). Using the same assumptions as before gives the equation

$$\frac{i}{i^{Ox}_{lim(R)}} = \frac{\left(1 + \exp\left[\frac{n^{Ox}_{sw}F(E - E^{Ox}_{sw})}{RT}\right]\right)^{-1}}{1 + \exp\left[\frac{n^{Ox}_{cat}F(E^{Ox}_{cat} - E)}{RT}\right]} \quad (7)$$

in which $i^{Ox}_{lim(R)}$ refers to the limiting oxidizing current for the enzyme in its reduced (i.e., active) form with respect to the high-potential switch. As shown in Figure 7, a good fit to the data at pH 9.0 was obtained with $E^{Ox}_{cat} = -112$ mV,

Table 2: Summary of the Molybdenum Potentials Determined by EPR

	E (Mo VI/V) (mV)	*E* (Mo V/IV) (mV)
pH 6.0	+63	−90
pH 7.0	0[a]	−138[a]
pH 8.0	−45	−155
pH 9.0	−83	−230

[a] These data are in good agreement with previously reported values (*13*, *14*).

$n_{cat}^{Ox} = 1.30 \pm 0.15$, and a *one*-electron switch ($n_{sw}^{Ox} = 1.0 \pm 0.1$) at $E_{sw}^{Ox} = -26$ mV. A summary of the parameters thus determined, which define a potential window of activity, is given in Table 1.

Figure 2 shows that the peak corresponding to an optimum potential for DMSO reduction lies at the same potential regardless of scan direction, i.e., there is no hysteresis. This was investigated further using scan rates up to 300 mV/s, for which both the catalytic and the switch potentials E_{cat}^{R} and E_{sw}^{R} were determined from the derivatives. Up to 50 mV/s, the values of E_{cat}^{R} and E_{sw}^{R} were independent of scan direction, whereas at high scan rates they separate at similar rates. This indicates that the catalytic and switch processes are occurring at comparable rates and supports the hypothesis (see below) that these two processes occur at the same center.

EPR Titrations. The reduction potentials of the Mo (VI/V) and (V/VI) couples have been measured previously at pH 7.0, both for the detergent-solubilized, purified enzyme and for the membrane preparation (*9*, *13*). The pH dependence of these potentials was measured between pH 6.0 and 9.0 for DmsABC in situ using a membrane preparation from cells overexpressing the enzyme. The EPR spectra obtained were identical to those described previously (*13*, *14*), with $g_1 = 1.984$, $g_2 = 1.980$, and $g_3 = 1.960$. The overall line shape of the Mo(V) signal is very similar to that of the high-pH form of nitrate reductase A (*47*) and the high-pH form of *Rh. sphaeroides* DMSOR (*48*). Fitting the intensity of the $g_2 = 1.980$ peak-trough versus potential to two E_m values corresponding to the Mo(VI/V) and Mo(V/VI) couples gives the values shown in Table 2. No significant change in line shape of the Mo(V) spectrum was observed between pH 6.0 and pH 9.0.

DISCUSSION

The experiments carried out with DmsABC reveal the characteristics of catalytic reduction of DMSO and TMAO, and, separately, the oxidation of PMe_3. Although we are uncertain how this complex enzyme is bound on the electrode, the results are very reproducible from sample to sample, and with variations in experimental conditions. A full profile of the activity as a function of potential (electronmotive driving force) can be developed. There is an unusual and striking potential dependence: in both reaction directions, the activity of the enzyme reaches a maximum activity, beyond which the rate drops back even though the thermodynamic driving force increases. Critical potentials can be assigned to processes that "switch" the enzyme off in each direction: these two switches are due to one-electron processes and separate three distinct states of the enzyme.

There are (at least) three possibilities for the potential dependence. First, it may be due to a redox transformation occurring at one of the centers in the enzyme. Second, there may be a potential-dependent change in the interaction of the protein with the electrode surface, leading to reorientation of the enzyme molecules and a concomitant change in efficiency of interfacial electron transfer. Third, the enzyme could be subject to product inhibition.

We have addressed the possibility of product inhibition in both the reduction and oxidation directions. In each case, introduction of an equimolar level of the respective product (DMS or $OPMe_3$) does not affect the form or magnitude of the current response. For the DMSO/DMS system, a 1000-fold excess of DMS can be added, yet DMSO reduction is unaffected. In the case of phosphine oxidation, it was not possible to achieve a high excess of product; however, 20 mM levels did not affect the voltammetry. Hence, in both cases we conclude that product inhibition is not responsible for the unusual potential dependence.

The possibility that the potential dependence is due to changes in the electrode interaction was also investigated. We were unsuccessful in obtaining voltammetry at a significantly different electrode surface such as gold, or observing a potential dependence of activity in solution (detecting such behavior in solution would, however, also depend on other factors such as control of solution potential, buffer composition, and ionic strength). However, several minor modifications to conditions (i.e., voltammetry at PGE or PGB electrodes, the presence and absence of a polymyxin coadsorbate, and different buffer systems) do not alter the current−potential profile.

The most likely explanation, therefore, is that the potential window relates to redox transitions of a group within the enzyme. The observations (i) that the redox switch occurs on the same time scale as catalysis, and (ii) that the voltammograms are fitted so well by a Nernstian expression, each support this proposal. Viewed by the voltammetric method, the effect is one of a "tunnel-diode", as observed previously for succinate dehydrogenase, in which a redox center functions also as a "switch" (*31*, *35*, *36*, *41*). Although DmsABC is a multicentered redox enzyme, the EPR data obtained from potentiometric titrations show that the best candidate for this switch is the Mo center. Figure 8, panel A, shows the results obtained for the EPR titration conducted at pH 9.0, expressed in terms of the fraction of Mo in the (V) oxidation state as a function of potential. In Figure 8, panel B, the resulting curve is superimposed on the electrochemical data for substrate oxidation and reduction, also at pH 9.0. Notwithstanding the differences in conditions under which these measurements were made (for example, the EPR titrations are carried out on membrane preparations in the absence of substrate, whereas the voltammetric data are obtained for detergent-solubilized enzyme under turnover conditions), there is a very striking correlation between the different data, with the region of optimum catalytic activity being centered on the potential region where Mo(V) predominates. Such a correlation provides compelling evidence for a special role for the Mo(V) state during catalysis.

A special role for the Mo(V) state can arise as follows. In the scheme depicted in Figure 9, electron-transfer steps (corresponding to reduction of the Mo cofactor) are arranged horizontally, with chemical steps appearing vertically. The

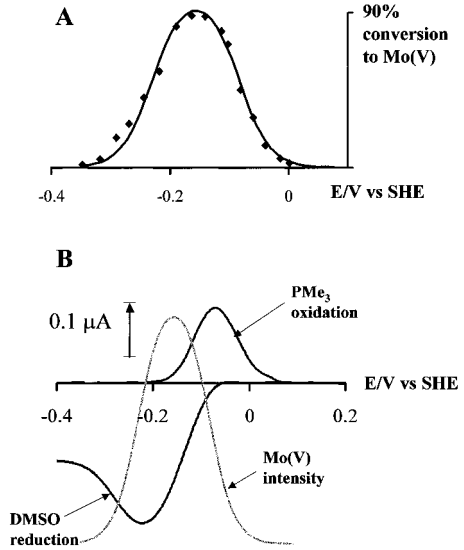

FIGURE 8: (A) Potentiometric titration of the Mo(V) signal from DmsABC-enriched membranes at pH 9.0. The intensity of the $g = 1.98$ peak-trough was plotted vs E_h and fitted to two $E_{m,9}$ values of −83 and −230 mV. The data are presented as the percentage conversion of the total Mo content to the Mo(V) state. (B) Baseline-subtracted voltammetric data for reduction of DMSO (pH 8.9) and oxidation of PMe_3 (pH 9.0), shown in black, both 20 mV/s. The gray line indicates the percentage of Mo in the V oxidation state, as shown in 8A.

chemical steps involve net proton transfer between enzyme and solvent, in accordance with the observed pH dependence of activity; however, it is important to stress that the actual sites of protonation cannot be identified by voltammetry alone. The necessary assumptions are that (i) each redox state of the cofactor exists in two forms, linked by the vertical transitions; (ii) these transitions involve protonations (Mo → Mo′-H) so that their rates increase as the pH is lowered; (iii) at sufficiently high pH, these vertical reactions become rate-limiting (although note this does not imply that elementary proton transfer is rate limiting); (iv) the rate of the vertical transition (Mo → Mo′-H^+) reaction is maximal for the Mo(V) state ($k_1^V > k_1^{IV}$). We also assume that the active site has to be fully reduced to the Mo(IV)′-H^+ state before the catalytic cycle is completed by reaction with DMSO, rate constant k_2.

The essential implication of the scheme is that the applied potential, by favoring particular redox states of the Mo active site, must direct the pathway taken between the Mo(VI) and the Mo(IV)′-H^+ states. Since the overall turnover rate depends on the rate of the limiting Mo → Mo′-H^+ reaction (fast for the Mo(V) state), the activity is optimized at an intermediate potential value, yielding the observed current peaks. At very low potentials, Mo(VI) is converted rapidly to Mo(IV), and the Mo(V) state does not accumulate; consequently, the critical Mo → Mo′-H conversion must occur in the Mo(IV) state, which is slower than for Mo(V), and hence the current drops to a lower plateau below the peak potential. Similarly, the rate-limiting step becomes slower at high pH since protons are required, which is reflected by the plot of limiting current vs pH, evaluated at low potential (Figure 3, panel A). Since the rates of the Mo → Mo′-H^+ reactions all increase as the pH is lowered, k_2 eventually becomes rate limiting at low pH. This results in the disappearance of the switch, since the pathway taken between Mo(VI) and Mo(IV)′-H^+ does not determine the rate of turnover. This is observed as a decrease in the ratio i^R_{peak}/i^R_{lim} as the pH is lowered, as illustrated in Figure 3, panel B.

This model accounts for the shapes of the voltammograms. The one-electron nature of the catalytic wave ($n^R_{cat} = 1$) results from the stability of the Mo(V) state (*33*) and shows that the most influential step in catalytic electron transport is reduction of Mo(V) to Mo(IV)-H^+. The value $n^R_{sw} = 1$ implicates the Mo(V) to Mo(IV) transformation as the origin of the switch. The steady-state solution gives an equation of the same form as eq 6 and shows that the expected value for E^R_{sw} is given by $E^R_{sw} = E^R_{cat} + RT/F \ln(k_1^{IV}/k_1^V)$. Since k_1^{IV} is lower than k_1^V (assumption iv), the switch is expected to occur at a lower potential than the Mo(V)/Mo(IV) transition, as observed in Figure 8, panel B. The actual values of E^R_{cat} and E^R_{sw} are therefore related to, but not equal to, the potential of the Mo(V)/(IV) couple, i.e., the apparent potential of the switch is not purely thermodynamic but depends on kinetics (i.e., the rate constants of the coupled processes). Additionally, this hypothesis is supported by the observation that the switch is a rapid process and that the rates of

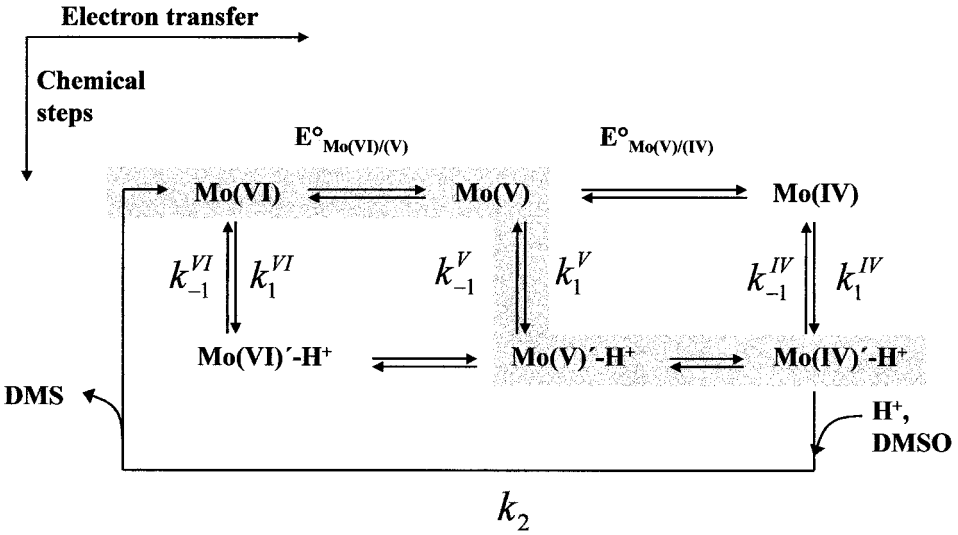

FIGURE 9: Proposed scheme for the catalytic cycle of DmsABC. The shaded box highlights the most efficient pathway for catalysis, which is taken at intermediate potentials where Mo(V) is dominant.

electron-transfer reactions involved in catalysis and the switch occur at comparable rates.

It is important to note that PFV, while allowing investigation of the energetics and kinetics of the catalytic process, offers only indirect evidence for species involved in the cycle. The pH dependences require that the vertical transitions shown in Figure 9 involve net transfer of a proton between enzyme and solvent, but it is certain that they are associated with more profound chemical processes, e.g., rearrangements. For example, the pH−activity profile (Figure 3, panel A), which is measured at low potential and corresponds to the rate of the vertical reaction from Mo(IV), shows activity falling off gradually over four pH units. This is not consistent with the vertical transition being a simple protonation step. Thus, the obvious complexity of the chemical processes accompanying the redox reactions in the scheme precludes any simple correlation with Mo coordination states. In this context, it is interesting to note observations made with another Mo-enzyme from *E. coli*, the membrane-bound respiratory nitrate reductase A (NarGHI) (*5*−*7*). In this enzyme, the Mo(V) EPR signal exists in two forms: a low-pH and high-pH form (*47*, *49*). It has been proposed that both these forms are involved in the catalytic cycle, with the protonation/deprotonation of Mo(V) occurring as an essential step in turnover (*49*). Changes in Mo(V) EPR spectra with pH are also observed for the relatively simple DMSO reductase from *Rh. sphaeroides* (*48*). In both these enzymes, it is clear that the molybdenum reduction potentials are much higher than those observed in DmsABC [*Rh. sphaeroides* DMSOR, +141/+160 mV at pH 7.0; *E. coli* nitrate reductase A, +95/+190 mV at pH 8.0 (*50*)]. However, our EPR results do not suggest any analogous changes occurring at the active site of DmsABC, so the pH dependence of activity must stem from a change that occurs outside the Mo coordination sphere.

The proposed model can explain accurately the shape of the wave at high pH, and the disappearance of the switch as the pH is decreased. Importantly, this same model equally applies to the oxidation of PMe_3 (following the cycle in the opposite direction). Again, the Mo(V) state dominates catalysis, but there is no appreciable reaction when the active site is oxidized to the Mo(VI) state, implying that the rate of the Mo(VI)′-H^+ → Mo(VI) reaction (k_{-1}^{VI}) is very slow. This suggests once more that the proton-linked reactions are complex and do not occur within the Mo coordination sphere, since the proton affinity of a simple Mo(VI) species should be very small and deprotonation should be fast.

Other redox-active groups that might be responsible for the "switch" are the Fe-S centers or the MGD moieties. Redox transformation of the Fe-S clusters may alter the rate of the catalytic reaction, as has been observed in *E. coli* fumarate reductase, for which potentials low enough to reduce the [4Fe-4S] cluster produce a boost in current (*32*), while a potential low enough to reduce the [3Fe-4S] cluster to the 2- level causes attenuation (*51*). However, the reduction potentials of the Fe−S clusters in DmsABC as measured by EPR (see Figure 1) do not coincide closely with the potentials of the switches. For the oxidative switch, the catalytic data are only available at pH 9.0, and strictly speaking, we cannot compare E_{sw}^{Ox} with the potentials of the Fe-S clusters determined at pH 7.0. The pterins may also be redox-active, and although these are expected to be two-electron reactions, a radical intermediate cannot be ruled out (*27*). Furthermore, recent reports on the reactivity of the dithiolene ligand have indicated that this group can dissociate (*25*) and undergo a redox reaction to give a thiyl radical (*28*) or a disulfide bridge (*24*). These possible redox reactions cannot be excluded, but spectroscopic studies have not yet suggested any such intermediates in the catalytic cycle; furthermore, it appears that loss of catalytic activity is associated with dissociation of thiolate ligands (*24*, *25*). Thus, while these species may be accessible, it seems unlikely that they are catalytically relevant.

In conclusion, our voltammetric studies of *E. coli* DMSO reductase show that catalytic activity is optimized within a narrow potential window, the boundaries of which each correspond to one-electron processes and coincide closely with the range of stability of Mo(V) as measured by EPR. This direct observation and the form of the voltammograms under different conditions are explained in terms of a reaction pathway that is *directed* through Mo(V), i.e., crucial steps in the mechanism, such as a rearrangement of atoms/groups in the active site are facilitated in this oxidation state. The results may have wider implications, e.g., for other molybdopterin enzymes, and raise further questions, as for succinate dehydrogenase, about whether the effects of such redox "switches" may be important for physiological regulation.

ACKNOWLEDGMENT

We thank Gillian Shaw for assistance with the enzyme preparations, Dr. Harsh Pershad for helpful discussions, and Theo Moore for conducting steady-state solution assays.

REFERENCES

1. Weiner, J. H., MacIsaac, D. P., Bishop, R. E., and Bilous, P. T. (1988) *J. Bacteriol. 170*, 1505−1510.
2. Sambasivarao, D., and Weiner, J. H. (1991) *Curr. Microbiol. 23*, 105−110.
3. Simala Grant, J. L., and Weiner, J. H. (1996) *Microbiol.-UK 142*, 3231−3239.
4. Simala Grant, J. L., and Weiner, J. H. (1998) *Eur. J. Biochem. 251*, 510−515.
5. Berg, B. L., Li, J., Heider, J., and Stewart, V. (1991) *J. Biol. Chem. 266*, 22380−22385.
6. Blasco, F., Iobbi, C., Giordano, G., Chippaux, M., and Bonnefoy, V. (1989) *Mol. Gen. Genet. 218*, 249−256.
7. Blasco, F., Iobbi, C., Ratouchniak, J., Bonnefoy, V., and Chippaux, M. (1990) *Mol. Gen. Genet. 222*, 104−111.
8. Sambasivarao, D., Turner, R. J., Simala Grant, J. L., Shaw, G., Hu, J., and Weiner, J. H. (2000) *J. Biol. Chem. 275*, 22526−22531.
9. Cammack, R., and Weiner, J. H. (1990) *Biochemistry 29*, 8410−8416.
10. Weiner, J. H., Rothery, R. A., Sambasivarao, D., and Trieber, C. A. (1992) *Biochim. Biophys. Acta 1102*, 1−18.
11. Rothery, R. A., and Weiner, J. H. (1996) *Biochemistry 35*, 3247−3257.
12. Trieber, C. A., Rothery, R. A., and Weiner, J. H. (1994) *J. Biol. Chem. 269*, 7103−7109.
13. Trieber, C. A., Rothery, R. A., and Weiner, J. H. (1996) *J. Biol. Chem. 271*, 27339−27345.
14. Rothery, R. A., Trieber, C. A., and Weiner, J. H. (1999) *J. Biol. Chem. 274*, 13002−13009.
15. McAlpine, A. S., McEwan, A. G., Shaw, A. L., and Bailey, S. (1997) *J. Biol. Inorg. Chem. 2*, 690−701.
16. Schindelin, H., Kisker, C., Hilton, J., Rajagopalan, K. V., and Rees, D. C. (1996) *Science 272*, 1615−1621.

17. Schneider, F., Lowe, J., Huber, R., Schindelin, H., Kisker, C., and Knablein, J. (1996) *J. Mol. Biol. 263*, 53−69.
18. McAlpine, A. S., McEwan, A. G., and Bailey, S. (1998) *J. Mol. Biol. 275*, 613−623.
19. Knablein, J., Dobbek, H., Ehlert, S., and Schneider, F. (1997) *Biol. Chem. 378*, 293−302.
20. Li, H.-K., Temple, C., Rajagopalan, K. V., and Schindelin, H. (2000) *J. Am. Chem. Soc. 122*, 7673−7680.
21. Garton, S. D., Hilton, J., Oku, H., Crouse, B. R., Rajagopalan, K. V., and Johnson, M. K. (1997) *J. Am. Chem. Soc. 119*, 12906−12916.
22. Garton, S. D., Temple, C. A., Dhawan, I. K., Barber, M. J., Rajagopalan, K. V., and Johnson, M. K. (2000) *J. Biol. Chem. 275*, 6798−6805.
23. George, G. N., Hilton, J., Temple, C., Prince, R. C., and Rajagopalan, K. V. (1999) *J. Am. Chem. Soc. 121*, 1256−1266.
24. Adams, B., Smith, A. T., Bailey, S., McEwan, A. G., and Bray, R. C. (1999) *Biochemistry 38*, 8501−8511.
25. Bray, R. C., Adams, B., Smith, A. T., Bennett, B., and Bailey, S. (2000) *Biochemistry 39*, 11258−11269.
26. Solomon, P. S., Lane, I., Hanson, G. R., and McEwan, A. G. (1997) *Eur. J. Biochem. 246*, 200−203.
27. Luykx, D. M., Duine, J. A., and de Vries, S. (1998) *Biochemistry 37*, 11366−11375.
28. Lane, I., Hanson, G. R., and McEwan, A. (1997) in *Molybdenum Enzymes Meeting*, pp P40, University of Sussex.
29. Armstrong, F. A., Heering, H. A., and Hirst, J. (1997) *Chem. Soc. Rev. 26*, 169−179.
30. Sucheta, A., Cammack, R., Weiner, J., and Armstrong, F. A. (1993) *Biochemistry 32*, 5455−5465.
31. Hirst, J., Sucheta, A., Ackrell, B. A. C., and Armstrong, F. A. (1996) *J. Am. Chem. Soc. 118*, 5031−5038.
32. Heering, H. A., Weiner, J. H., and Armstrong, F. A. (1997) *J. Am. Chem. Soc. 119*, 11628−11638.
33. Heering, H. A., Hirst, J., and Armstrong, F. A. (1998) *J. Phys. Chem. B 102*, 6889−6902.
34. Armstrong, F. A., Butt, J. N., and Sucheta, A. (1993) *Methods Enzymol. 227*, 479−500.
35. Hirst, J., Ackrell, B. A. C., and Armstrong, F. A. (1997) *J. Am. Chem. Soc. 119*, 7434−7439.
36. Pershad, H. R., Hirst, J., Cochran, B., Ackrell, B. A. C., and Armstrong, F. A. (1999) *Biochim. Biophys. Acta-Bioenerg. 1412*, 262−272.
37. Rothery, R. A., and Weiner, J. H. (1991) *Biochemistry 30*, 8296−8305.
38. Condon, C., and Weiner, J. H. (1988) *Mol. Microbiol. 2*, 43−52.
39. Rothery, R. A., Chatterjee, I., Kiema, G., McDermott, M. T., and Weiner, J. H. (1998) *Biochem. J. 332*, 35−41.
40. Bard, A. J., and Faulkner, L. R. (1980) *Electrochemical Methods- Fundamentals and Applications*, John Wiley & Sons, New York.
41. Sucheta, A., Ackrell, B. A. C., Cochran, B., and Armstrong, F. A. (1992) *Nature 356*, 361−362.
42. Jones, A. K., Turner, K. L., Chapman, S. K., and Armstrong, F. A. (1999) *J. Inorg. Biochem. 74*, 183.
43. Wood, P. M. (1981) *FEBS Lett. 124*, 11−14.
44. Bach, R. D., Winter, J. E., and McDouall, J. J. W. (1995) *J. Am. Chem. Soc. 117*, 8586−8593.
45. Finklea, H. O. (1996) in *Electroanalytical Chemistry* (Bard, A. J., Ed.) pp 109−335, Dekker, New York.
46. Ackrell, B. A. C., Armstrong, F. A., Cochran, B., Sucheta, A., and Yu, T. (1993) *FEBS Lett. 326*, 92−94.
47. Vincent, S. P., and Bray, R. C. (1978) *Biochem. J. 171*, 639−647.
48. Bastian, N. R., Kay, C. J., Barber, M. J., and Rajagopalan, K. V. (1991) *J. Biol. Chem. 266*, 45−51.
49. Magalon, A., Asso, M., Guigliarelli, B., Rothery, R. A., Bertrand, P., Giordano, G., and Blasco, F. (1998) *Biochemistry 37*, 7363−7370.
50. Rothery, R. A., Magalon, A., Giordano, G., Guigliarelli, B., Blasco, F., and Weiner, J. H. (1998) *J. Biol. Chem. 273*, 7462−7469.
51. Heffron, K. (2000) unpublished results.

BI002452U